Available online at www.sciencedirect.com
SCIENCE DIRECT
Journal of Power Sources 156 (2006) 211–223
JOURNAL OF POWER SOURCES
www.elsevier.com/locate/jpowsour

Computational study of water transport in proton exchange membrane fuel cells

Sukkee Um [a,*], Chao-Yang Wang [b]

[a] *Fuel Cell Research Center, Korea Institute of Energy Research, P.O. Box 103, Yuseong, Daejeon 305-600, Republic of Korea*
[b] *Electrochemical Engine Center, Department of Mechanical and Nuclear Engineering, The Pennsylvania State University, University Park, PA 16802, USA*

Received 25 February 2005; accepted 23 May 2005
Available online 22 August 2005

Abstract

A computational fuel cell dynamics framework is used to develop a unified water transport equation for a proton exchange membrane fuel cell (PEMFC). Various modes of water transport, i.e., diffusion, convection and electro-osmotic drag, are incorporated in the unified water transport equation. The water transport model is then applied to elucidate water management in three-dimensional fuel cells with dry-to-low humidified inlet gases after its validation against available experimental data for dry oxidant and fuel streams. An internal circulation of water with the aid of counter-flow design is found to be of vital importance for low-humidity operation, for example, in the portable application of a PEMFC without an external humidifier. The general features of water transport in PEMFCs are discussed to show various water transport regimes of practical interest, such as anode water loss, cathode flooding, and the equilibrium condition of water at the channel outlets, particularly for limiting situations where anode and cathode water profiles acquire an equilibrium state. From the practical point of view, the effects of the flow arrangement, membrane thickness, and inlet gas humidity as important determinants of fuel cell performance are also analyzed to elucidate fuel cell water transport characteristics.

Keywords: Proton exchange membrane fuel cell; Computational study; Water transport

1. Introduction

In the previous modelling efforts of proton exchange membrane fuel cells (PEMFCs) [1–4], the ionomer membrane remained fully humidified, which yields a constant proton conductivity and minimum ohmic loss. Under such operating conditions, however, the gas phase is over-saturated with water vapour and water condensation may occur on the cathode side even at low operating current densities. The ensuing cathode flooding by liquid water subsequently hinders the access of oxygen to the cathode catalyst layer and results in significant concentration polarization. In addition, full humidification of the reactant gases externally involves parasitic volume and power losses in the fuel cell system. Therefore, it is of practical interest to operate PEMFCs under low-humidity conditions, while still maintaining the polymer electrolyte membrane adequately hydrated. Such low-humidity operating strategies will also reduce cathode flooding and space requirement for auxiliary equipment to a minimum extent. Obviously, such an innovative operating scheme hinges upon a good understanding of water generation, transport, and distribution within PEMFCs.

The research presented here is dedicated to studying water transport and distribution in PEMFCs by extending the computational fuel cell dynamics (CFCD) model developed by Um et al. [5]. A key challenge in applying a unified CFCD framework to describe water transport is to recognize the fact that there are different phases of water existing in various regions of a PEMFC, i.e. water in the gas phase and in the membrane. As a result, phase equilibrium must be considered. Furthermore, various modes of water transport,

* Corresponding author. Tel.: +82 42 806 3542; fax: +82 42 860 3309.
E-mail address: sukkeeum@kier.re.kr (S. Um).

0378-7753/$ – see front matter © 2005 Elsevier B.V. All rights reserved.
doi:10.1016/j.jpowsour.2005.05.095

Nomenclature

a	effective catalyst area per unit volume ($cm^2\ cm^{-3}$) or water activity
c	molar concentration ($mol\ cm^{-3}$)
D	mass diffusivity of species ($cm^2\ s^{-1}$)
EW	equivalent weight of membrane
I	current density ($A\ cm^{-2}$)
j	transfer current ($A\ cm^{-3}$)
n_d	electro-osmotic drag coefficient
P	pressure (Pa)
R	gas constant, $8.314\ J\ mol^{-1}\ K^{-1}$
t	time (s)
T	temperature (K)
u	velocity vector ($cm\ s^{-1}$)
U	inlet velocity at gas channel
V	potential (V)
y	axial location

Greek letters

ζ	stoichiometric flow ratio (Eq. (1))
κ	ionic conductivity ($S\ m^{-1}$)
ρ	density ($kg\ cm^{-3}$)

Subscripts

a	anode
c	cathode
crit	critical water loss in the anode
e	electrolyte
fl	cathode flooding
g	gas diffusion layer
ref	reference value
W	water

Superscripts

eff	effective value
g	gas phase
m	membrane phase
sat	saturation value

i.e., diffusion, convection and electro-osmotic drag, must be incorporated in the unified water transport equation. An equilibrium water uptake curve in the membrane phase [1] is thus introduced to extend the existing CFCD framework to various low membrane humidification conditions.

Water is produced at the cathode catalyst layer as a result of the oxygen reduction reaction (the product water) and can be brought into the cell by humidified reactant gases. The various modes of water transport through the membrane electrolyte, primarily the electro-osmotic drag effect and diffusion driven by the concentration gradient, are illustrated in Fig. 1. The water flux due to electro-osmotic drag is directly proportional to the proton flux (I_{cell}/F); the proportionality constant is called the 'electro-osmotic drag coefficient', n_d. The diffusion flux of water in the membrane is usually described by a water diffusion coefficient and by the gradient of molar concentration of water.

A number of excellent computational efforts on water management in PEMFCs have been made [6–10] to account for multiple water transport modes across die proton exchange membrane. Some approaches solve a simplified one-dimensional water transport model [6,7,11], other computational works excluded the thin catalyst layer or treat it as an interface [8–10,12]. A significant contribution to analysing water transport in PEMFCs has been made by Zawodzinski et al. [13–15] and Springer et al. [1,16], both experimentally and computationally.

Zawodzinski et al. [13–15] conducted a series of experiments on the sorption characteristics of Nafion® membrane. They measured water uptake by a membrane in equilibrium with liquid water and water vapour, and estimated die electro-osmotic drag coefficient for various membrane water contents. A coefficient of unity for membranes equilibrated with water vapour over a wide range of water activities was determined experimentally. Ren and Gottesfeld [17] showed the effects of temperature, membrane hydration level, membrane equivalent weight and membrane type on the electro-osmotic drag coefficient. They found that the drag coefficient is independent of the cell current density.

A diffusion model was introduced by Springer et al. [1] for a Nafion® 117 membrane, which included the electro-osmotic drag term. They assumed an equilibrium between the gas phase and the membrane phase of water in the Nafion® membrane, and then determined the membrane water content at the interface from the activity of water vapour. Hsing and Futerko [9] developed a two-dimensional, finite element based model for a PEMFC without external humidification of the inlet gas streams. The flow field was approximated using a potential flow equation with a stream function. The membrane water content at the anode vertical line membrane interface was calculated under the assumption of phase equilibrium between the vapour and the membrane phases, and the cathode vertical line membrane interface was taken to be fully hydrated. More recently, Janssen [10] demonstrated one- and two-dimensional numerical models to account for water transport through the membrane electrode assembly (MEA) under various humidification conditions of inlet gases. Computed results were compared with experimental data measured by Janssen and Overvelde [18]. In this model, it is assumed that the cell current density is constant everywhere, and the catalyst layers are excluded in the water transport calculation. Reacting species along the channel and in the through-membrane direction of the MEA are calculated based on the assumption of one-dimensional mass transport.

In the present work, a unified water transport equation within the single-domain CFCD framework is developed with the aid of the equilibrium water uptake curve in the membrane phase. Emphasis is placed on how to derive correctly the unified water transport equation with the various transport modes incorporated. Also, this water

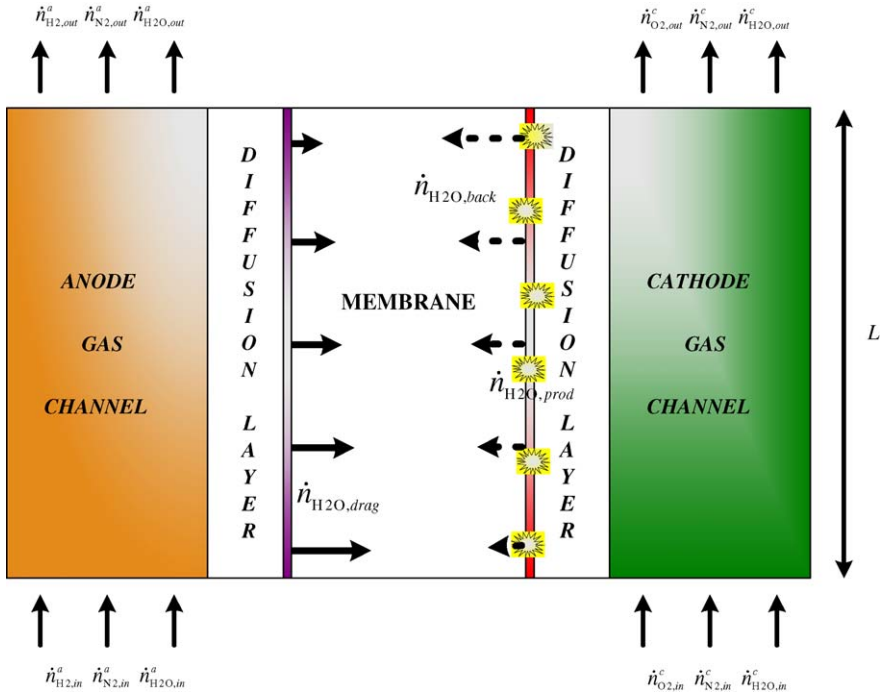

Fig. 1. Schematic diagram of water transport mechanism in fuel cell domain.

transport model is validated against available experimental data from the literature, and then applied to elucidate water management in three-dimensional fuel cells with low humidified inlet reactant gases.

2. Characteristics of water concentration profiles in anode and cathode

The general features of water transport in a fuel cell domain are schematically shown in Fig. 1. Water leaves the anode under the electro-osmotic drag when an electrical potential is applied, while water is driven back from the cathode to the anode by the concentration gradient that primarily arises from water production at the cathode catalyst layer. Water loss on the anode surface of the membrane caused by the electro-osmotic drag becomes significant at large current densities and the back-diffusion of water usually becomes stronger along the axial direction as depicted in Fig. 1.

Typical water concentration profiles in the anode and cathode along the flow direction are depicted in Fig. 2. The water concentration at the anode vertical line membrane interface decreases along the axial direction and then reaches the minimal point at which the net water flux across the membrane becomes zero. This implies that the electro-osmotic drag is balanced by the back-diffusion of water. The location, y_{crit} in Fig. 2 indicates this zero net water flux location. Before this critical location, the anode is characterized by water loss, while after the location the anode gains water. In the worst situation, the anode can be fully dehydrated if the back-diffusion from the cathode is not sufficiently strong to compensate for the loss of anode water by electro-osmotic drag. This critical location is also important in that it signifies the most resistive location of the membrane.

For current densities greater than a certain value, so much water is produced at the cathode that the gas is saturated with water vapour and a vapour-to-liquid phase change is imminent, which brings about cathode flooding. Theoretically, liquid water appears at a flooding point, y_{fl}, shown in Fig. 2.

When a thin membrane is used in a fuel cell, the water exchange between the anode and cathode is greatly facilitated. Thereby, the water concentrations on the anode and cathode sides of the membrane approach each other towards the exit, a state called the 'equilibrium of water'. This is depicted as curve C1 in Fig. 2. This equilibrium condition occurs only when the back-diffusion of water through the membrane is largely dominating. If, however, the membrane is sufficiently thick that back-diffusion of water cannot compensate for the electro-osmotic drag of water from the anode to cathode, the differential in water concentration between the anode and the cathode will widen as a result of water production on the cathode side. This is shown as curve C2 in Fig. 2.

3. CFCD model for water transport

For this water transport study, a multi-dimensional CFCD model developed by Um et al. [5] is extended to model accurately water transport and distribution in a PEMFC, as shown

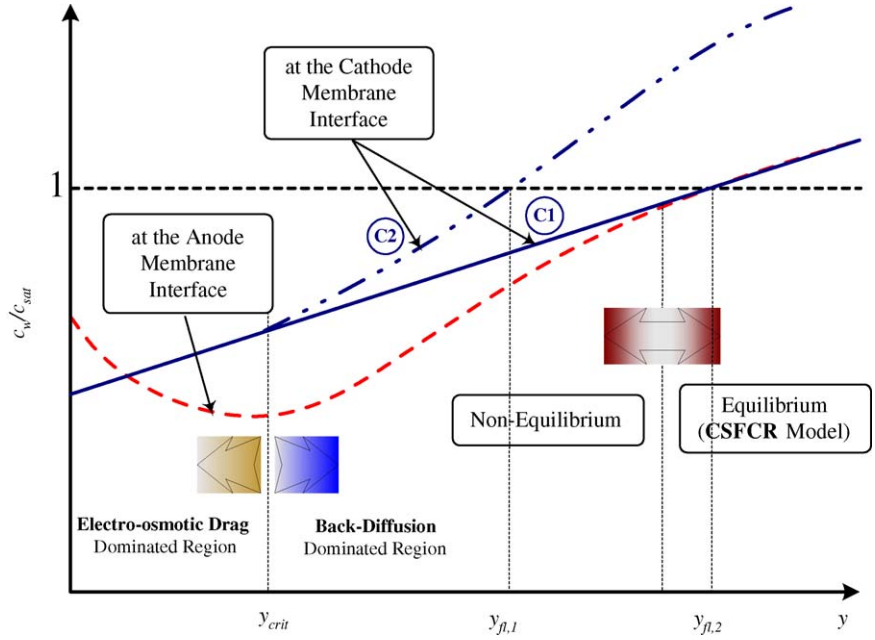

Fig. 2. Graphical representation of water concentration profiles along flow direction in both anode and cathode of co-flow design, showing various regimes of water transport.

in Fig. 3, particularly for low-humidity operation in which the anode and the cathode inlet gases are only slightly humidified.

A distinguishing feature of the present CFCD model lies in its unified treatment of water transport throughout all regions of a fuel cell. The model how the single species equation for water presented in the previous work [5] can describe all transport modes in various regions.

3.1. Flow channels and backing layers

When applied to water, the species conservation equation for water reduces to the following for flow channels and backing layers:

$$\frac{\partial(\varepsilon c_{\mathrm{W}}^{\mathrm{g}})}{\partial t} + \nabla \cdot (\varepsilon \vec{u} c_{\mathrm{W}}^{\mathrm{g}}) = \nabla \cdot (D_{\mathrm{W}}^{\mathrm{eff}} \nabla c_{\mathrm{W}}^{\mathrm{g}}) \tag{1}$$

where ε is the porosity of the gas channel and the backing layer; $c_{\mathrm{W}}^{\mathrm{g}}$ the water molar concentration in gas phase; $\vec{u}$ the intrinsic fluid velocity and $D_{\mathrm{W}}^{\mathrm{eff}}$ is an effective mass diffusivity defined in the previous study [5].

The physical meaning of Eq. (1) is apparent, each term has a unit of (mol m^{-3} s^{-1}). An effective transport property for the porous region is modified from its intrinsic physical property by a Bruggemann factor [5].

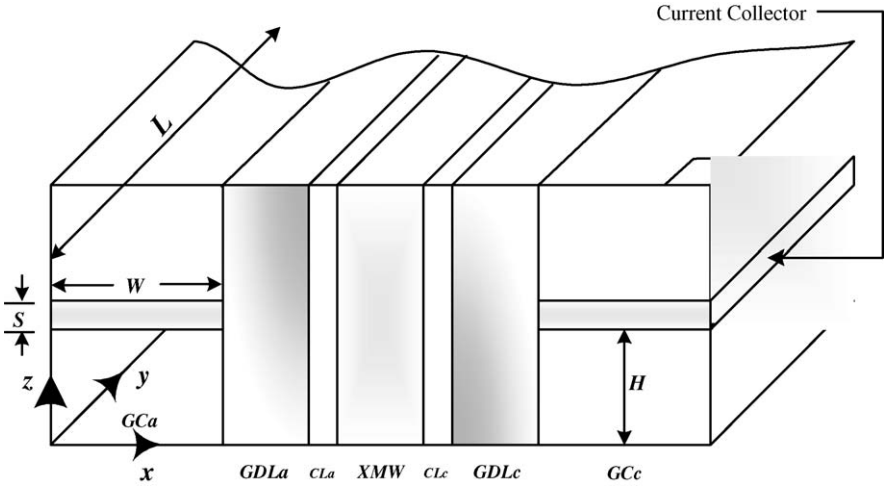

Fig. 3. Description of cell geometry of PEMFC.

3.2. Membrane

The general water transport equation reduces to the following:

$$\frac{\partial(\varepsilon c_{\mathrm{W}}^{\mathrm{g}})}{\partial t} = \nabla\cdot(D_{\mathrm{W}}^{\mathrm{g}}\nabla c_{\mathrm{W}}^{\mathrm{g}}) - \frac{1}{F}\nabla\cdot(n_{\mathrm{d}} I_{\mathrm{e}}) \tag{2}$$

for the membrane region. Here, use has been made of the assumption that fluid velocity is zero in the membrane. In Eq. (2), the water molar concentration, $c_{\mathrm{W}}^{\mathrm{g}}$, is a fictitious vapour concentration ($c_{\mathrm{W}}^{\mathrm{g}} = (P_{\mathrm{sat}}/RT_{\mathrm{cell}})a$) that is in thermodynamic equilibrium with a membrane of water content λ (or its equivalent membrane water concentration, $c_{\mathrm{W}}^{\mathrm{m}} = (\rho_{\mathrm{dry}}/\mathrm{EW})\lambda$). The one-to-one correspondence between $c_{\mathrm{W}}^{\mathrm{g}}$ and $c_{\mathrm{W}}^{\mathrm{m}}$ can be called the 'equilibrium uptake curve', as shown in Fig. 4(a).

The main advantage of using the fictitious gas-phase water concentration, $c_{\mathrm{W}}^{\mathrm{g}}$, in the membrane region is to ensure continuity of the variable field across the electrode vertical line membrane interface, as shown in Fig. 4(b). The solid line represents a physical variable, whereas the dashed line denotes a fictitious quantity that is solved in the numerical program

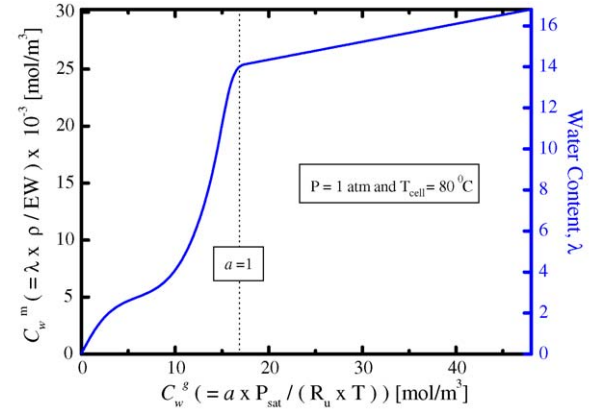

(a)

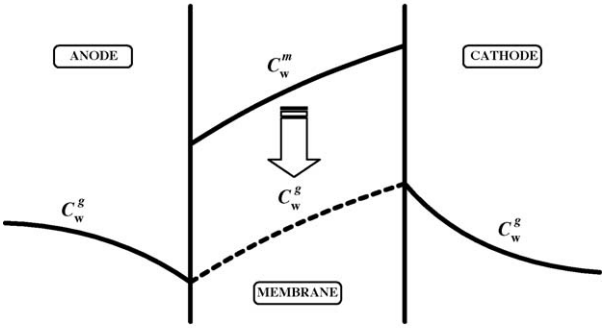

(b)

Fig. 4. (a) Equilibrium uptake curves for Nafion® membrane relating membrane water concentration to equilibrium gas phase water concentration (created from Springer et al. [1] relation between the water content and activity) and (b) schematic profiles of water concentrations in various regions of a PEMFC.

in order to obtain the physically meaningful variable more conveniently.

The diffusion coefficient for $c_{\mathrm{W}}^{\mathrm{g}}$ in the membrane region is thus equal to:

$$D_{\mathrm{W}}^{\mathrm{g}} = D_{\mathrm{W}}^{\mathrm{m}}\frac{\mathrm{d}c_{\mathrm{W}}^{\mathrm{m}}}{\mathrm{d}c_{\mathrm{W}}^{\mathrm{g}}} = D_{\mathrm{W}}^{\mathrm{m}}\frac{1}{\mathrm{EW}}\frac{RT}{P_{\mathrm{sat}}}\left(\rho + \lambda\frac{\mathrm{d}\rho}{\mathrm{d}\lambda}\right)\frac{\mathrm{d}\lambda}{\mathrm{d}a} \tag{3}$$

where the derivatives, $\mathrm{d}\rho/\mathrm{d}\lambda$ and $\mathrm{d}\lambda/\mathrm{d}a$, can be evaluated from ρ–λ and λ–a property correlations. Substituting the expression for $D_{\mathrm{W}}^{\mathrm{g}}$, Eq. (3), into Eq. (2) results in Springer's model [1] of water transport through the membrane under steady-state:

$$\nabla\cdot(D_{\mathrm{W}}^{\mathrm{m}}\nabla c_{\mathrm{W}}^{\mathrm{m}}) - \frac{1}{F}\nabla\cdot(n_{\mathrm{d}} I_{\mathrm{e}}) = 0 \tag{4}$$

or

$$\nabla\cdot\left(D_{\mathrm{W}}^{\mathrm{m}}\frac{\rho_{\mathrm{dry}}}{\mathrm{EW}}\nabla\lambda\right) - \frac{1}{F}\nabla\cdot(n_{\mathrm{d}} I_{\mathrm{e}}) = 0 \tag{5}$$

if the membrane density is assumed to be constant (i.e., no membrane swelling is considered).

Therefore, the water transport equation used in the present model unifies the water transport process in the gas phase with that in the membrane, and thereby permits a single-domain simplification in computations. A salient feature of this unified water transport equation is the fact that the water flux intrinsically remains continuous across the interface between the gas-diffusion electrode and the membrane. This water flux continuity is not automatically guaranteed in many previous models using a multi-domain approach.

A comment is in order on the effect of the electro-osmotic drag on water transport through the membrane phase. It follows from Eq. (5) that this effect is directly proportional to the gradient of the ionic current, $\nabla\cdot I_{\mathrm{e}}$.

Various expressions of the electro-osmotic drag coefficient, n_{d}, have been proposed in the literature; for example,

$$n_{\mathrm{d}} = \begin{cases} \dfrac{2.5\lambda}{22} & \text{(a)} \\ \left[\dfrac{1}{(0.35\lambda)^4} + \dfrac{1}{1.47^4}\right]^{-1/4} & \text{(b)} \\ 1 & \text{(c)} \end{cases} \tag{6}$$

The electro-osmotic drag coefficient expression given by Springer et al. [1] has a linear dependence on the water content, as expressed by Eq. (6a), whereas Fuller [19] determined the water drag coefficient by Eq. (6b). On the other hand, the experimentally measured proton transport number of water shows a constant value close to 1.0 for a water content level up to 14, while for a membrane immersed in liquid water, the water drag by protons has an abrupt discontinuity and jumps to 2.5 H_2O/H^+ [15]. In the present study, the constant electro-osmotic drag coefficient given in Eq. (6c) is used for computational purpose.

Table 1
Water transport equation in various regions of fuel cell

Components	Governing equation	Diffusivity
Anode gas channel		$D_{\mathrm{W}}^{\mathrm{g}}$
Anode backing layer		$\varepsilon_{\mathrm{g}}^{1.5} D_{\mathrm{W}}^{\mathrm{g}}$
Anode catalyst layer		$\varepsilon_{\mathrm{c}}^{1.5} D_{\mathrm{W}}^{\mathrm{g}} + (\varepsilon_{\mathrm{m}})^n D_{\mathrm{W}}^{\mathrm{m}}$
Membrane	$\frac{\partial(\varepsilon c_{\mathrm{W}})}{\partial t} + \nabla \cdot (\varepsilon \vec{u} c_{\mathrm{W}}) = \nabla \cdot (D^{\mathrm{eff}} \nabla c_{\mathrm{W}}) + S_{\mathrm{W}}$	$D_{\mathrm{W}}^{\mathrm{m}}$
Cathode catalyst layer		$\varepsilon_{\mathrm{c}}^{1.5} D_{\mathrm{W}}^{\mathrm{g}} + (\varepsilon_{\mathrm{m}})^n D_{\mathrm{W}}^{\mathrm{m}}$
Cathode backing layer		$\varepsilon_{\mathrm{g}}^{1.5} D_{\mathrm{W}}^{\mathrm{g}}$
Cathode gas channel		$D_{\mathrm{W}}^{\mathrm{g}}$

3.3. Catalyst layers

Water transport is through both gas and membrane phases in catalyst layers. Assuming that the water diffusion paths through the gas and membrane phases are in parallel, the total diffusive flux as follows:

$$N_{\mathrm{W}} = \varepsilon_{\mathrm{c}}^{1.5}(-D_{\mathrm{W}}^{\mathrm{g}} \nabla c_{\mathrm{W}}^{\mathrm{g}}) - (\varepsilon_{\mathrm{m}})^n D_{\mathrm{W}}^{\mathrm{m}} \frac{\mathrm{d}c_{\mathrm{W}}^{\mathrm{m}}}{\mathrm{d}c_{\mathrm{W}}^{\mathrm{g}}} \nabla c_{\mathrm{W}}^{\mathrm{g}} = -D_{\mathrm{W}}^{\mathrm{eff}} \nabla c_{\mathrm{W}}^{\mathrm{g}} \tag{7}$$

where

$$D_{\mathrm{W}}^{\mathrm{eff}} = \varepsilon_{\mathrm{c}}^{1.5} D_{\mathrm{W}}^{\mathrm{g}} + D_{\mathrm{W}}^{\mathrm{m}} \frac{\mathrm{d}c_{\mathrm{W}}^{\mathrm{m}}}{\mathrm{d}c_{\mathrm{W}}^{\mathrm{g}}} \tag{8}$$

Note that water diffusion is practically through the gas phase in the catalyst layer because the water diffusion coefficient in the membrane phase is roughly two orders of magnitude smaller than the gas phase.

The unified water transport equation is summarized in Table 1 along with its diffusivity expressions in various regions of the PEMFC. More information on general governing equations and source/sink terms for fuel cell modelling is given by Um et al. [5].

3.4. Boundary conditions

At the fuel and oxidant inlets, the following conditions are prescribed:

$$\begin{aligned} u_{\mathrm{in,anode}} &= U_{\mathrm{a,in}}, \qquad u_{\mathrm{in,cathode}} = U_{\mathrm{c,in}}, \\ c_{\mathrm{H_2,anode}} &= c_{\mathrm{H_2,a}}, \qquad c_{\mathrm{O_2,cathode}} = c_{\mathrm{O_2,c}}, \\ c_{\mathrm{H_2O,anode}} &= c_{\mathrm{H_2O,a}}, \qquad c_{\mathrm{H_2O,cathode}} = c_{\mathrm{H_2O,c}} \end{aligned} \tag{9}$$

The inlet velocities of fuel and oxidant can also be expressed by their respective stoichiometric flow ratios, i.e., ζ_{a} and ζ_{c} at 1 A cm^{-2}. At the outlets, both anode and cathode channels are assumed to be sufficiently long so that velocity and species concentration fields are fully developed.

3.5. Numerical procedures

The conservation equations [5] were discretized using a finite volume method [20] and were solved using a general-purpose computational fluid dynamic (CFD) code. Details of the numerical solution procedure and the code have been given in previous work [5]. Stringent numerical tests were performed to ensure that the solutions were independent of the grid size. A $50 \times 100 \times 60$ mesh (or, about 300,000 elements) was found to provide sufficient spatial resolution. The coupled set of equations was solved iteratively, and the solution was considered to be convergent when the relative error in each field between two consecutive iterations was less than 10^{-5}.

4. Results and discussion

This section focuses on applying the unified water transport model to three-dimensional fuel cells. This enables the investigation of water transport phenomena and its effect on the cell performance. A series of three-dimensional simulations are performed, including both anode and cathode gas streams with full humidification (AFCF), fully humidified anode flow but dry cathode flow (AFCD), both anode and cathode with low humidification (i.e., RH = 20%) (ALCL), and both anode and cathode with dry gases (ADCD). The focus of these simulations is on the prediction of water content profiles across the ionomer membrane as well as the resulting current density distribution.

The feed stream in the anode gas channel is assumed to consist of hydrogen and water vapour only to simulate direct-hydrogen fuel cell vehicles, while air is supplied to the cathode (i.e., oxygen, nitrogen, and water vapour).

It is assumed that the amount of Pt catalyst and its transfer current density within the catalyst layer remain the same in all simulation cases. The physical and transport properties and the electrochemical kinetics are summarized in Tables 2 and 3. The basic operating conditions and the cell design parameters are summarized in Tables 4 and 5.

4.1. Experimental validation

To validate the unified water transport model developed here, a special application of fuel cells operated under no humidity is considered. The computed polarization curve and the water removal rate through the anode channel are compared in Fig. 5 with the published experimental data of Büchi

Table 2
Electrochemical kinetics

Description	Anode	Cathode
Reference cell potential, Φ_{s} (V)	0	V_{cell}
Equilibrium potential, V_0 (V) [22]	$V_{\mathrm{a,0c}} = 0$	$V_{\mathrm{c,0c}} = 0.0025T + 0.2329$
Exchange current density × reaction surface area, aj_0^{ref} (A m^{-3})	1.0×10^9	$2 \times 10^4 \exp[0.014189(T - 353)]$
Transfer coefficient, α	$\alpha_{\mathrm{a}} + \alpha_{\mathrm{c}} = 2$	$\alpha_{\mathrm{c}} = 1$
Faraday constant, F (C)	96487	

Table 3
Transport properties

Property	Value	Reference
Ionic conductivity of membrane, κ (S m^{-1})	$(0.5139\lambda - 0.326)\exp\left[1268\left(\frac{1}{303} - \frac{1}{T}\right)\right]$	[1]
H_2O diffusion coefficient in membrane, D_W^m (m^2 s^{-1})	$D_W^m = \begin{cases} 3.1\times10^{-7}\lambda(e^{0.28\lambda}-1)\,e^{-2346/T} & \text{for } 0<\lambda\le 3 \\ 4.17\times10^{-8}\lambda(1+161\,e^{-\lambda})\,e^{-2346/T} & \text{otherwise} \end{cases}$	[23]
H_2 diffusivity in gas, D_{H_2} (m^2 s^{-1})	$1.1\times10^{-4}\left(\frac{T}{353}\right)^{3/2}\left(\frac{1}{P}\right)$	[24]
O_2 diffusivity in gas, D_{O_2} (m^2 s^{-1})	$3.2\times10^{-5}\left(\frac{T}{353}\right)^{3/2}\left(\frac{1}{P}\right)$	[24]
H_2 diffusivity in membrane, $D_{H_2}^m$ (m^2 s^{-1})	2.59×10^{-10}	[3]
O_2 diffusivity in membrane, $D_{O_2}^m$ (m^2 s^{-1})	1.22×10^{-10}	[3]
H_2O diffusivity in gas, D_{H_2O} (m^2 s^{-1})	$7.35\times10^{-5}\left(\frac{T}{353}\right)^{3/2}\left(\frac{1}{P}\right)$	[24]

Table 4
Basic operating conditions

Description	Symbol	Value
Cell temperature	T_{cell}	80 °C
Operating cell voltage	V_{cell}	–
Pressure at gas channel inlet of anode side	P_a	2.0 atm
Hydrogen mole fraction at anode gas channel inlet	$c^a_{H_2,in}$	–
Water vapour mole fraction at anode gas channel inlet	$c^a_{W,in}$	–
Stoichiometry ratio in anode gas channel	ζ_a	2.0
Pressure at gas channel inlet of cathode side	P_c	2.0 atm
Oxygen mole fraction at cathode gas channel inlet	$c^c_{O_2,in}$	–
Nitrogen mole fraction at cathode gas channel inlet	$c^c_{N_2,in}$	–
Water vapour mole fraction at cathode gas channel inlet	$c^c_{W,in}$	–
Stoichiometry ratio in cathode gas channel	ζ_c	2.0

and Srinivasan [21] that was intended to apply an internally humidified mechanism to a portable power application by controlling the water balance. The calculated curves show good agreement with the measured experimental data for the polarization curve, and also predict the general trends of the removal rate of water collected at the anode outlet as a function of the hydrogen flow stoichiometry.

Having validated the present CFCD model in cases without external humidification, the following discussion involves the general features of water transport and parametric studies to gain a better understanding of the optimum water balance over a fuel cell by varying such parameters as the anode

Table 5
Design parameters

Description	Symbol	Value
Cell/electrode length	L	7.36 cm
Gas channel height	H	0.159 cm
Gas channel width	W	0.254 cm
Current collector width	S	0.082 cm
Anode GDL thickness	GDL_a	0.02 cm
Porosity of anode GDL	ε_a	0.4
Anode catalyst layer thickness	CL_a	0.001 cm
Porosity of anode catalyst layer	ε_{CL_a}	0.112
Membrane thickness	XMW	
Cathode catalyst layer thickness	CL_c	0.001 cm
Porosity of cathode catalyst layer	ε_{CL_c}	0.112
Porosity of cathode GDL	ε_c	0.4
Cathode GDL thickness	GDL_c	0.02 cm

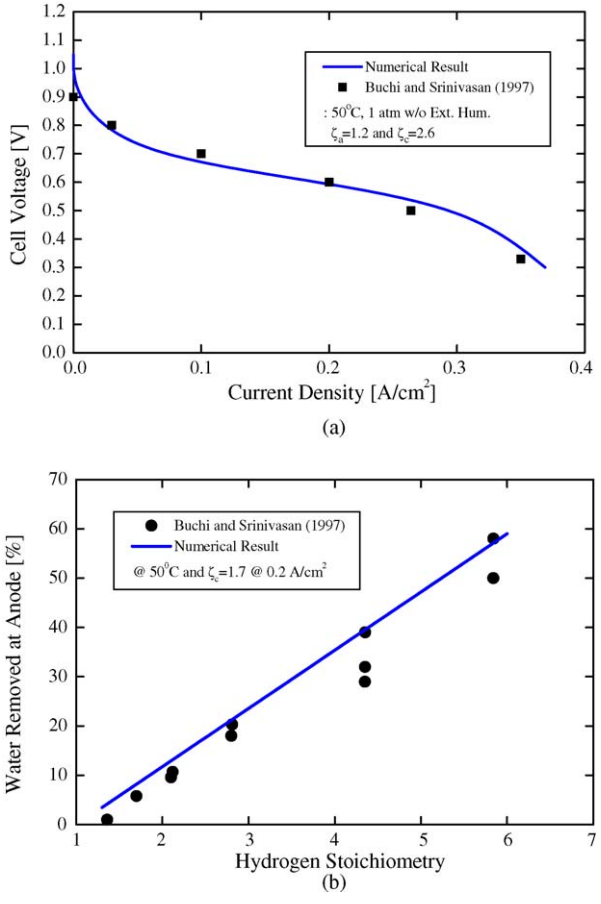

Fig. 5. (a) Experimental and computed polarization curves for fuel cell without external humidification and (b) percent of water removed through anode channel outlet as function of hydrogen stoichiometry for problem described in Fig. 7, and comparison of experimental with numerical results.

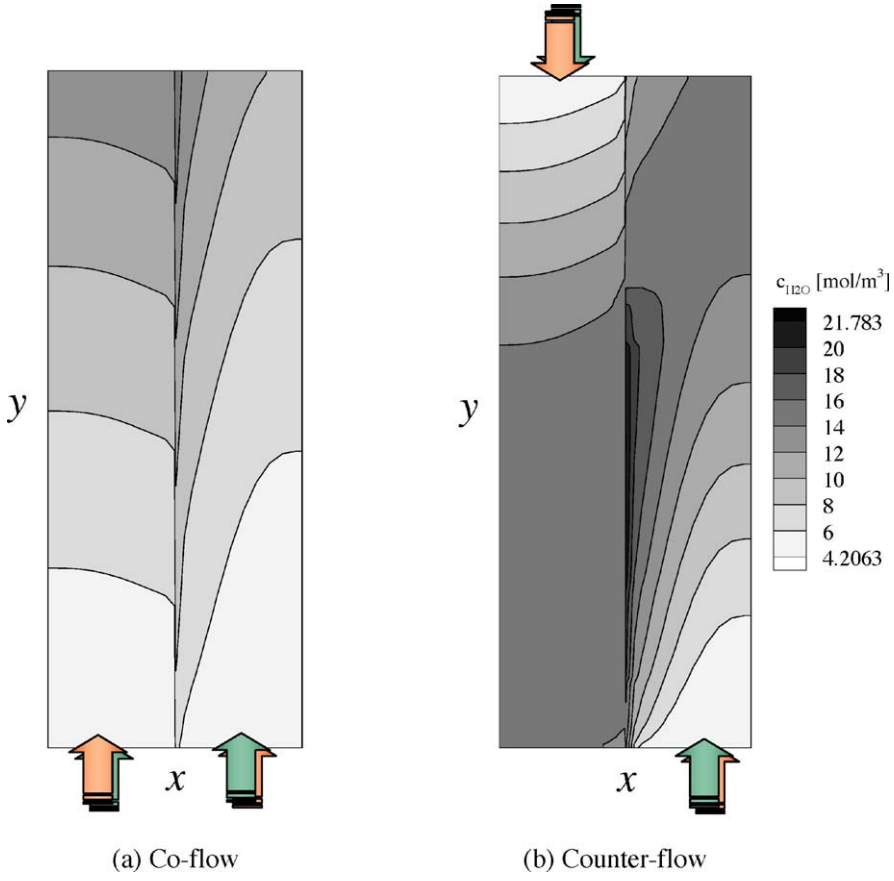

Fig. 6. Water molar concentration distribution in fuel cell: ALCL, Nafion® 111, 0.6 V, and $z = H/2$. Left channel is for anode and right channel for cathode.

and cathode flow directions, membrane thickness, and inlet humidity values.

4.2. Anode and cathode flow arrangement

The predicted two-dimensional water concentration contours on the x–y plane at $z = H/2$ are shown in Fig. 6 for the ALCL (RH = 20%) case in the co-flow and the counter-flow designs of the anode and cathode, respectively. In the co-flow channel, water is transported from the cathode to the anode along the entire gas channel (i.e., one-way water flux), while in the counter-flow design, water crosses through the membrane from anode to cathode up to the mid-length along the channel (i.e. $y = L/2$), and then water goes back from cathode to anode above the mid-length (i.e., two-way water flux) as shown in Fig. 6.

The internal circulation of water resulting from the two-way water flux through the membrane is a unique feature of the counter-flow design and causes the electrolyte membrane hold more water for better ionic conductivity. This is evident in Fig. 7, which shows the calculated water content profiles across the membrane thickness at three representative y-locations along the gas channel. In the co-flow design, the water content increases monotonously with the axial direction. Due, however, to the internal circulation of water flux created by the counter-flow design, the water content reaches a maximum value in the mid-portion of the fuel cell (i.e., $y = L/2$), while at both ends of the fuel cell the membrane contains less water, as can be seen in Figs. 6(b) and 7.

There is an increase of at least 30% in the predicted cell current density for the counter-flow design at $V_{cell} = 0.6$ V. This is ascribed to the internal circulation pattern of water flow over the entire cell domain with a thin membrane (e.g., Nafion® 111). By contrast, there is a negligible effect of the

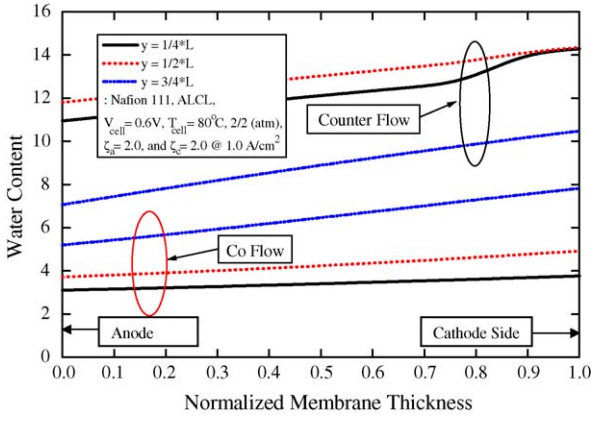

Fig. 7. Water content profiles at selected y-points: Nafion® 111, ALCL, 0.6 V, and $z = H/2$.

Table 6
The effect of operating parameters on the overall cell performance

V_{cell} (V)	(Nafion® 117) (I_{avg}, A cm^{-2})				(Nafion® 111) (I_{avg}, A cm^{-2})			
	ADCD		ALCL (RH = 20%)		ADCD		ALCL (RH = 20%)	
	Co-flow	Counter-flow	Co-flow	Counter-flow	Co-flow	Counter-flow	Co-flow	Counter-flow
0.4	0.107	0.108	0.260	0.271	1.251	1.384	1.337	1.352
0.6	0.037	0.037	0.126	0.127	0.399	0.590	0.799	1.069

flow direction on the cell performance with Nafion® 117 when dry gases or the low humidification of the inlet gases are supplied as shown in Table 6.

4.3. Effect of membrane thickness

The predicted water concentration contours for Nafion® 117 and Nafion® 112 membranes on the x–y plane at $z = H/2$ show very similar patterns of water transport under the full humidification of inlet gases in the counter-flow design, as illustrated in Fig. 8. A greater production rate of water is expected on the cathode side of Nafion® 112 membrane, due to the lower ionic resistance of the membrane compared with that of the thicker Nafion® 117 membrane. Through the anode gas channel, the enhanced back-diffusion of water in a thin membrane offsets the water loss by the electro-osmotic drag, as shown in Fig. 8. The predicted water content profiles across the normalized membrane thickness are given in Fig. 9, in which zero refers to the anode vertical line membrane interface and unity for the cathode vertical line membrane interface. The water content level for Nafion® 117 and Nafion® 112 at the cathode vertical line membrane interface is almost the same. On the other hand, there is a large difference in the water content at the anode vertical line membrane interface, which demonstrates the effect of the membrane thickness on the pack-diffusion of water.

The predicted local current density contours on the y–z plane for Nafion® 117 and Nafion® 112 are presented in Fig. 10 under the same operating conditions as above. A thinner membrane yields more current due to its lower ionic resistance. In addition, the improved water back-transport for the thinner Nafion® 112 membrane apparently has a

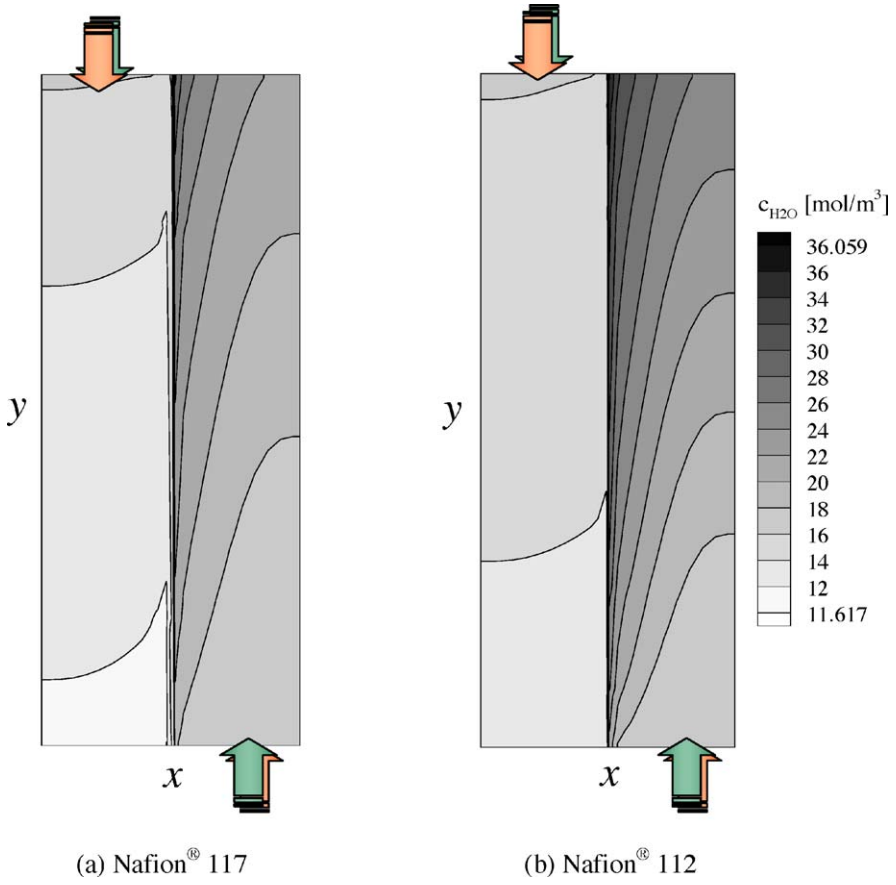

(a) Nafion® 117 (b) Nafion® 112

Fig. 8. Water molar concentration over fuel cell domain: counter-flow, AFCF, 0.6 V, and $z = H/2$.

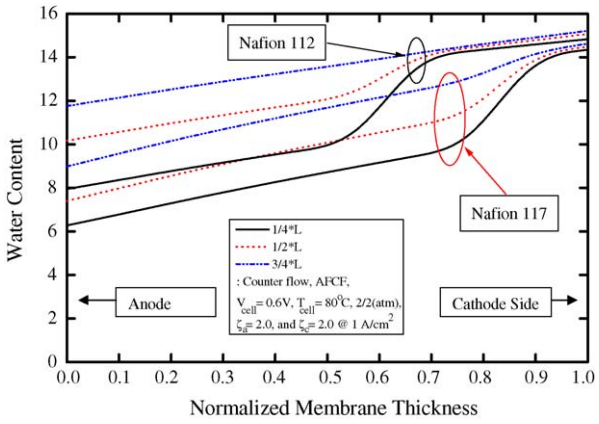

Fig. 9. Water content profiles at selected y-points: counter-flow, AFCF, 0.6 V, and $z = H/2$.

positive effect on the cell performance, as shown in Fig. 10. As discussed above, well-hydrated membrane shows good ionic conductivity which is a function of water content in the electrolyte phase. For Nafion® 117, the local current density has an almost flat profile over the entire reaction area and is low compared with Nafion® 112 at the same cell voltage, $V_{cell} = 0.6$ V. In general, a thick membrane always

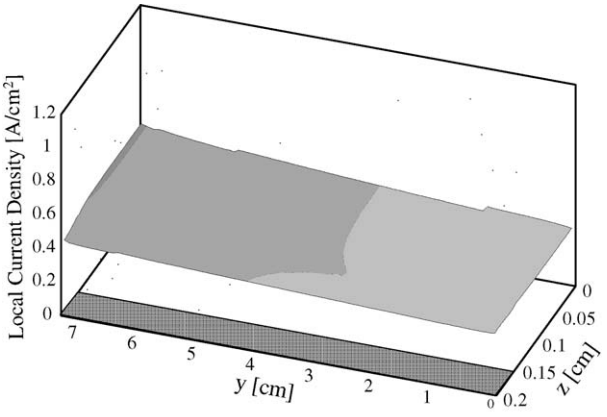

(a) Nafion® 117

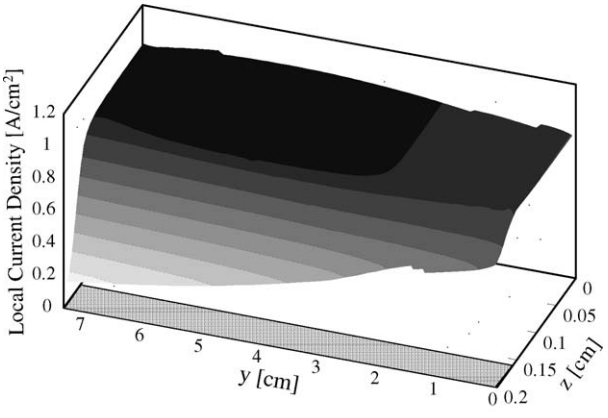

(b) Nafion® 112

Fig. 10. Local current density distribution: counter-flow, AFCF at 0.6 V.

produces a more uniform current density distribution. By contrast, in a thin membrane, higher local current densities are predicted within the catalytic reaction zone parallel to the gas chamber, which signifies a large oxidant consumption. Therefore, a lower available amount of oxidant results in lower current densities at the reaction area underneath the current-collector rib in Fig. 10(b) than the minimum local current density in a thick membrane, as shown in Fig. 10(a).

4.4. Effect of inlet gas humidity

The predicted two-dimensional contours of the water concentration on the x–y plane at $z = H/2$ over the entire fuel cell of Nafion® 111 at $V_{cell} = 0.6$ V for ADCD and ALCL (RH = 20%) cases are presented in Fig. 11. Under dry hydrogen and dry air inlet conditions, it can be seen from Fig. 11(a) that the water concentration remains below the saturation level (i.e., 16.14 mol m^{-3}) and results in low ionic conductivity of the electrolyte. Conversely, adding a slight amount of water vapour (i.e., RH = 20%) helps the PEMFC retain a considerable amount of water over the entire cell geometry, as illustrated, in Fig. 11(b). The maximum water concentration at the cathode vertical line membrane interface in Fig. 11(b) becomes greater than the saturation water concentration, i.e., 16.14 mol m^{-3}, at 80 °C under 2 atm.

Computed profiles of water content are presented in Fig. 12 for selected y-locations along the gas channel under the same operating conditions as for Fig. 11. In the ADCD case, the water content λ has a constantly low value (i.e., approximately $\lambda = 3$) across the membrane due to its small thickness (Nafion® 111). The low current output due to the large ionic resistance of the dry membrane, and therefore an insufficient water production rate, cannot produce a high water content in the membrane. For ALCL (RH = 20%) case, however, the water content level on the cathode membrane interface exceeds the saturation value (i.e., λ = 14) and there is also a significant amount of water at the anode vertical line membrane interface in Fig. 12, which suggests that water diffuses smoothly back from the cathode to the anode.

The predicted local current density contours on the y–z plane for Nafion® 111 in the counter-flow design are shown in Fig. 13 for operating conditions of $V_{cell} = 0.6$ V, 80 °C, and 2 atm for ADCD and ALCL (RH = 20%) cases, respectively. As discussed earlier, the thinner Nafion® 111 membrane generally enhances the back-diffusion of water. The dry fuel and dry air inlet streams are not enough, however, to cause a sufficient water concentration in the cell and thus a conductive membrane for high rate of water production. The end result is a low cell current density. On the contrary, slight humidification (e.g., RH = 20%) of the inlet fuel and air gases helps to induce a positive chain-effect, namely, it increases the water concentration level so as to provide good membrane conductivity, improves the current output, and intensifies water production within the cell.

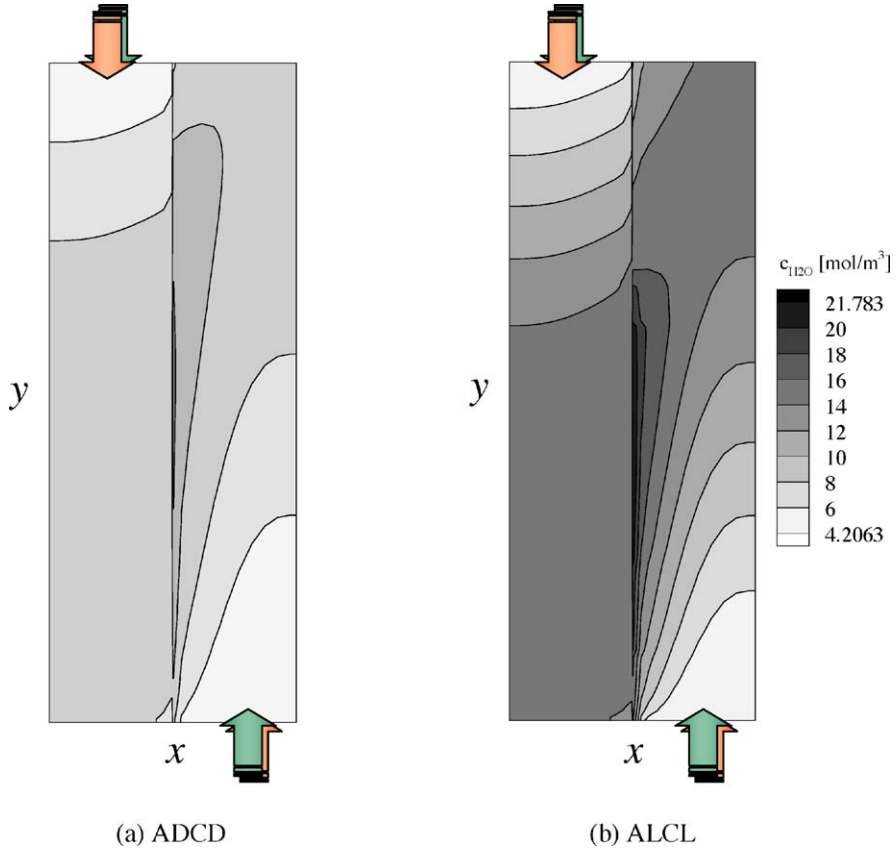

(a) ADCD (b) ALCL

Fig. 11. Water molar concentration: Nafion® 111, counter-flow, 0.6 V, and $z = H/2$.

4.5. High performance regime of low-humidity operation

Calculated water content profiles in the membrane are given in Fig. 14 for selected y-locations along the gas channel of Nafion® 112 at $z = H/2$ and $V_{cell} = 0.6$ V for various humidification cases, viz., RH = 20, 50 and 100%. The lowest humidification of the inlet gas streams (RH = 20%) contains a significantly low amount of water in the membrane, which results in considerable ionic resistance across the ionomer membrane. The low cell current density, owing to this large ionic resistance, cannot produce sufficient water by the cathode catalytic reaction. With moderate humidification (RH = 50%), however, the water content level in the membrane is equivalent to that of full humidification of the inlet gases (RH = 100%). The water content at the cathode vertical membrane interface reaches the saturation value (i.e., $\lambda = 14$) and there is also a significant amount of water at the anode vertical membrane interface, as shown in Fig. 14. This results in a high cell current density comparable with that for full humidification (RH = 100%).

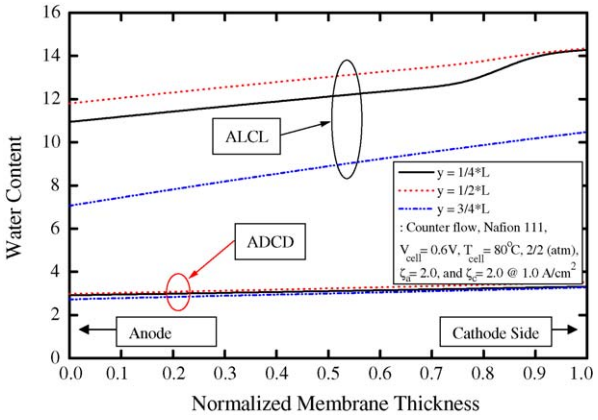

Fig. 12. Water content profiles at selected y-points: counter-flow, Nafion® 111, 0.6 V, and $z = H/2$.

4.6. Polarization curves

Computed performance curves for the co- and counter-flow of Nafion® 112 under the basic operating conditions are presented in Fig. 15. Three distinctive characteristics are worth noting. First, with anode humidification only (AFCD), it is possible to achieve a level of performance as much as that obtained with full humidification of both anode and cathode gases (AFCF). This finding is of significant practical importance because it is easier to humidify the anode gas, due to its much smaller flow rate, than the cathode air.

Second, either dry supply (ADCD) or low humidification (ALCL) of inlet flows yield significantly lower performance than the AFCF and AFCD cases at high cell voltage of

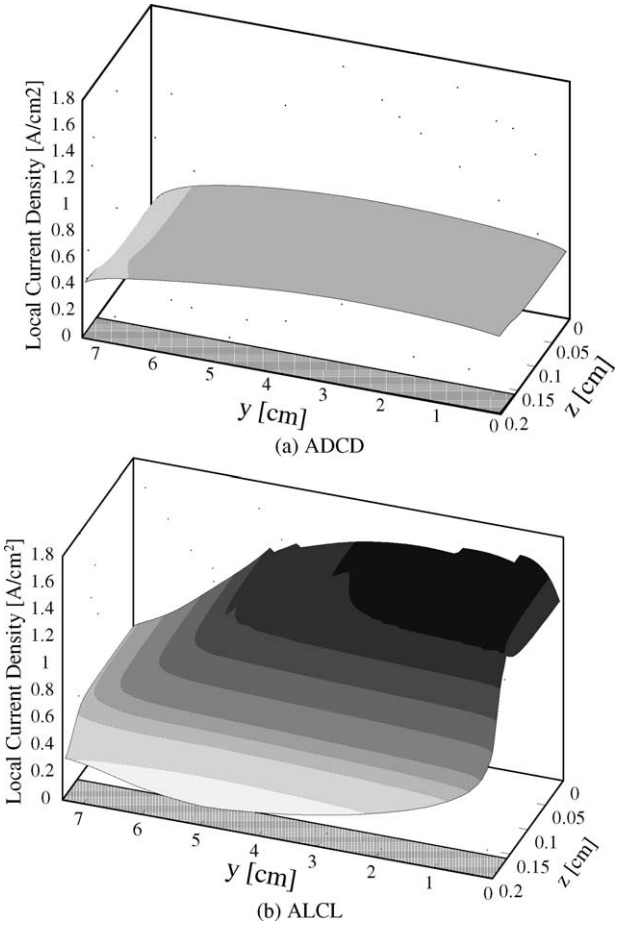

Fig. 13. Local current density distribution of Nafion® 111: counter-flow at 0.6 V.

$V_{cell} = 0.6$ V. As mentioned above, however, the performance is much improved as the cell voltage is reduced. The third point is evident from Fig. 15(b), that is, dry hydrogen and dry air feed streams (ADCD) in the co-flow design cannot sustain a high current density at even low cell voltages. This suggests that it would be more suitable to adopt a counter-flow design to achieve the high current density comparable

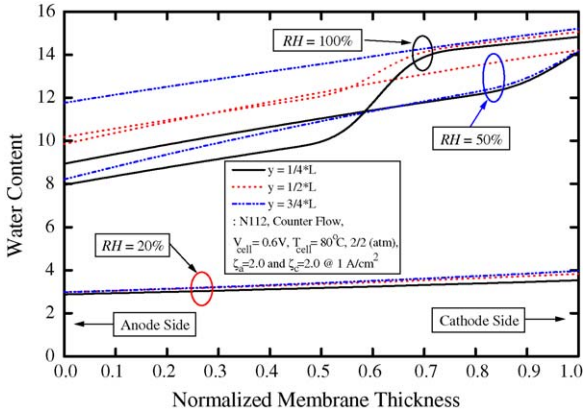

Fig. 14. Water content profiles at selected y-points: counter-flow, Nafion® 112, 0.6 V, and $z = H/2$.

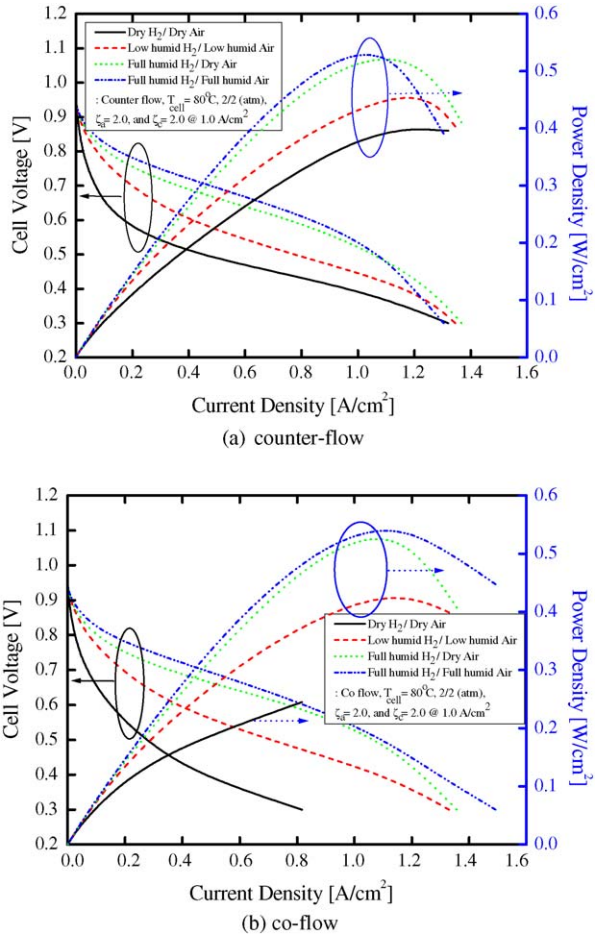

Fig. 15. Polarization and power density curves for Nafion® 112 membrane.

with the full humidification case at low cell voltage with a loss of less than 15% of the maximum power density, as shown in Fig. 15(a).

5. Conclusions

A unified water transport CFCD model based on the single-domain approach has been developed to account for various water transport modes in the electrolyte and to provide a convenient tool to assess water distribution in PEMFCs that have different humidification strategies. The effects of flow arrangement, membrane thickness, and inlet gas humidity on fuel cell performance have been analyzed to elucidate the water transport characteristics. It is demonstrated that thicker membranes yield not only higher ohmic resistances but also less back-diffusion flux of water across the membrane. It is also found that low humidification of inlet gases can produce a cell current density equivalent to full humidification at low cell voltages and/or with a counter-flow design. The latter design creates internal water circulation, which facilitates membrane hydration. Finally, a fuel cell unit using dry inlet gases could be an alternative power source

for portable electronics provided that the internal water circulation can be utilized to eliminate need for any external humidification.

References

[1] T.E. Springer, T.A. Zawodzinski, S. Gottesfeld, Electrochem. Soc. 136 (1991) 2334–2342.
[2] D.M. Bernardi, M.W. Verbrugge, AIChE J. 37 (1991) 1151–1163.
[3] D.M. Bernardi, M.W. Verbrugge, J. Electrochem. Soc. 139 (1992) 2477–2491.
[4] T. Berning, D.M. Lu, N. Djilali, J. Power Sources 106 (2002) 284–294.
[5] S. Um, C.Y. Wang, K.S. Chen, J. Electrochem. Soc. 147 (2000) 4485–4493.
[6] T. Okada, G. Xie, O. Gorseth, S. Kjelstrup, N. Nakamura, T. Arimura, Electrochim. Acta 43 (1998) 3741–3747.
[7] T. Okada, G. Xie, M. Meeg, Electrochim. Acta 43 (1998) 2141–2155.
[8] P. Futerko, I.-M. Hsing, Electrochim. Acta 45 (2000) 1741–1751.
[9] I.-M. Hsing, P. Futerko, Chem. Eng. Sci. 55 (2000) 4209–4218.
[10] G.J.M. Janssen, J. Electrochem. Soc. 148 (2001) A1313–A1323.
[11] H. Voss, D.D. Wilkinson, P. Pickup, M. Johnson, V. Basura, Electrochim. Acta 40 (1995) 321–328.
[12] N. Djilali, D.M. Lu, Int. J. Therm. Sci. 41 (2002) 29–40.
[13] T.A. Zawodzinski, C. Derouin, S. Radzinski, R. Sherman, V.T. Smith, T.E. Springer, S. Gottesfeld, J. Electrochem. Soc. 140 (1993) 1041–1048.
[14] T.A. Zawodzinski, T.E. Springer, F. Uribe, S. Gottesfeld, Solid State Ionics 60 (1993) 199–211.
[15] T.A. Zawodzinski, J. Davey, J. Valerio, S. Gottesfeld, Electrochim. Acta 40 (1995) 297–302.
[16] T.E. Springer, M.S. Wilson, S. Gottesfeld, J. Electrochem. Soc. 140 (1993) 3513–3527.
[17] X. Ren, S. Gottesfeld, J. Electrochem. Soc. 148 (2001) A87–A93.
[18] G.J.M. Janssen, M.L. Overvelde, J. Power Sources 101 (2001) 117–125.
[19] T.F. Fuller, Ph.D. Thesis, University of California, Berkeley, USA, 1992.
[20] S.V. Patankar, Numerical Heat Transfer and Fluid Flow, Hemisphere, New York, USA, 1980.
[21] F.N. Büchi, S. Srinivasan, J. Electrochem. Soc. 144 (1997) 2767–2773.
[22] A. Parthasarathy, S. Srinivasan, A.J. Appleby, J. Electrochem. Soc. 139 (1992) 2530–2538.
[23] S.W. Yeo, A. Eisenberg, J. Appl. Polym. Sci. 21 (1977) 875–898.
[24] R.H. Perry, D.W. Green, J.O. Maloney, Perry's Chemical Engineers' Handbook, McGraw-Hill, New York, USA, 1984.